Lithographically directed self-assembly of nanostructures

J. Alexander Liddle[a)]
Materials Sciences Division, Lawrence Berkeley National Laboratory, Room 2-419, 1 Cyclotron Road, Berkeley, California 94720-8232

Yi Cui and Paul Alivisatos
Department of Chemistry, University of California, Berkeley,California and Materials Sciences Division, Lawrence Berkeley National Laboratory, Room 2-419, 1 Cyclotron Road, Berkeley, California 94720-1460

(Received 16 September 2004; accepted 27 September 2004; published 14 December 2004)

The combination of lithography and self-assembly provides a powerful means of organizing solution-synthesized nanostructures for a wide variety of applications. We have developed a fluidic assembly method that relies on the local pinning of a moving liquid contact line by lithographically produced topographic features to concentrate nanoparticles at those features. The final stages of the assembly process are controlled first by long-range immersion capillary forces and then by the short-range electrostatic and van der Waals interactions. We have successfully assembled nanoparticles from 50 to 2 nm in size using this technique and have also demonstrated the controlled positioning of more complex nanotetrapod structures. We have used this process to assemble Au nanoparticles into prepatterned electrode structures and have performed preliminary electrical characterization of the devices so formed. The fluidic assembly method is capable of very high yield, in terms of positioning nanostructures at each lithographically defined location, and of excellent specificity, with essentially no particle deposition between features. © *2004 American Vacuum Society.* [DOI: 10.1116/1.1821572]

INTRODUCTION

Nanostructures synthesized in solution, such as colloidal metal nanocrystals[1,2] and semiconductor quantum dots,[3,4] nanorods,[5] and nanotetrapods,[6] can have precisely controlled sizes in the range of 1 to 100 nm and exhibit behaviors distinct from those of nanostructures fabricated by vacuum deposition or lithography. They have applications in electronics,[7] magnetics,[8] and photonics.[9] Their high degree of uniformity and relative ease of production means that they are promising building units for nanotechnology. This promise will not be fulfilled, however, unless methods of positioning and addressing these units individually can be developed.

Previous efforts in this area have consisted primarily of lithographic patterning followed by random deposition,[10,11] or electrostatic,[12] or magnetic[13] trapping of nanostructures. These approaches do not provide precise positioning, require specific susceptibilities, have typically low throughput, and/or are not amenable to scaling. We have developed a simple fluidic method for reproducibly fabricating large-scale arrays which incorporate controlled numbers of spherical or complex-shape colloidal nanocrystals at precise, lithographically determined locations on a chip and within a circuit. In contrast to previously described fluidic assembly processes,[14,15] our method yields structures with minimal dependence on the direction of fluid flow, is highly specific, and is compatible with relatively sparse lithographic features and with low-concentration nanoparticle suspensions.

In this article we will discuss the mechanism of the self-assembly process and describe our recent results.

a)Electronic mail: jaliddle@lbl.gov

FORCES ON NANOPARTICLES

At this point it is worth reviewing the forces that act on a nanoparticle in solution in order to determine which might prove suitable for assembling the nanoparticles at lithographically-defined features. We require a force that: can overcome the Brownian motion or thermal energy of the particles; is long range; is localized at the lithographic feature; and is capable of retaining the particle at the feature once the fluid has evaporated. For particles smaller than about 1 μm in diameter, gravitational/buoyancy forces may be neglected, having a magnitude (for a 1 μm Au particle in water) of 10^{-3} nN. These may be compared to the thermal energy kT by calculating the work done on a particle in moving it, for example, a distance equal to its diameter. For a nominal 10 nm Au particle the gravitational/buoyancy work becomes equivalent to a negligible 10^{-11} kT.

Electrostatic forces can be quite substantial and, in the absence of screening effects, are certainly long range. The actual magnitudes are highly dependent on experimental conditions such as pH and ionic concentration. At the lower end, a SiO_2 surface in pH 7 water might have a surface charge of 10^{-4} to 10^{-3} e^-/nm^2,[16] exerting an unscreened force of order 100 fN on a point charge, while for a highly charged material, the surface charge might be 0.8 e^-/nm^2, with a corresponding force of order 100 pN. The potential energy of two 10 nm Au particles with a typical surface potential of 20 to 125 mV,[17] and including the relevant screening effects,[18] is a few kT. The screening length is typically of the order 10 to 100 nm.[17]

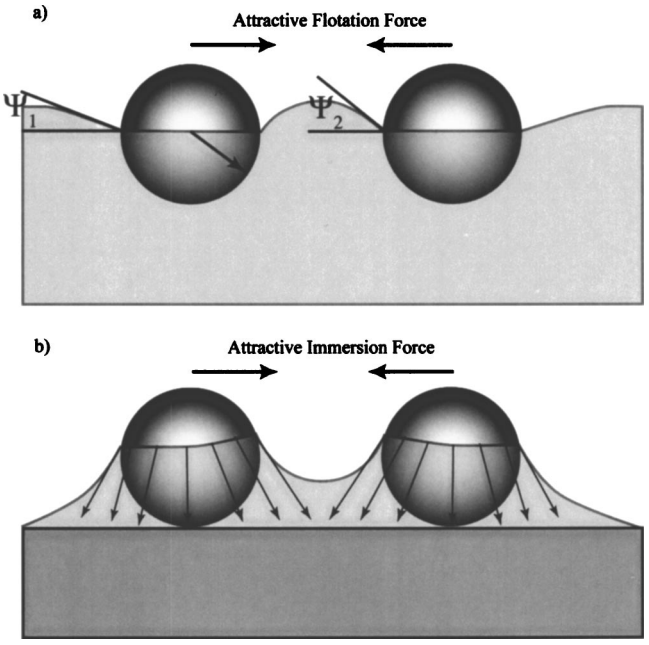

FIG. 1. (a) Origin of flotation capillary forces. The meniscus is deformed leading to a difference in the meniscus slope angles Ψ_1 and Ψ_2. Note that these forces become negligible for particles smaller than a few micrometers in size. (b) Origin of immersion capillary forces. Integration of the horizontal component of the surface tension around the contact lines produces a net attractive force between the particles. Note that these remain significant, even for particles as small as two nanometers. [After Kralchevsky and Nagayama (Ref. 19)].

The van der Waals interaction energy between two particles of diameter D, separated by distance d, is given approximately by

$$\Delta W_{\text{van der Waals}} \approx AD/24d, \tag{1}$$

where A is the Hamaker constant (2.5×10^{-19} J for Au in water).[17] For two 10 nm Au particles in water at a separation of 2 nm this energy is again equivalent to a few kT. We note that the electrostatic and van der Waals energies must be comparable at small inter-particle separations for the colloid to be stable.

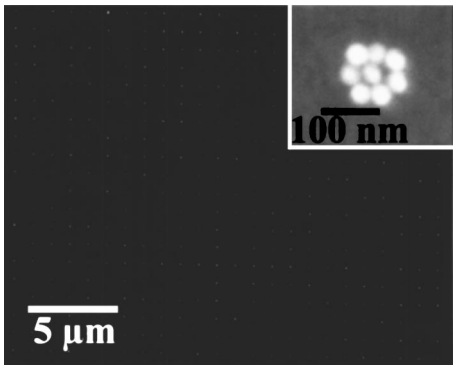

FIG. 2. SEM micrograph showing the assembly of 50 nm Au particles into 150 nm, 1 μm pitch holes in KRS-XE resist. The inset shows the typical arrangement of particles within a single hole. The particles are concentrated by a factor of 10^4–10^5 relative to the concentration of the suspension. Note that there are essentially no particles deposited between the lithographically defined features.

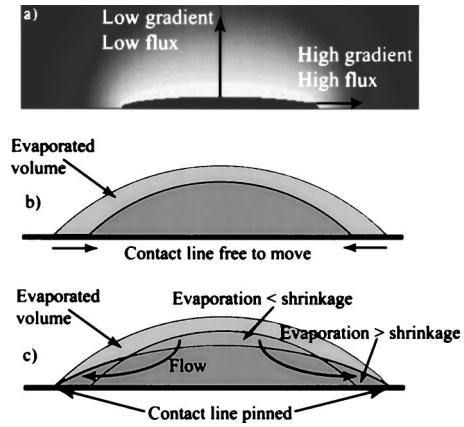

FIG. 3. (a) Illustration of vapor concentration as a function of position (white-high, black-low) over an oblate spheroid. This solution does not exhibit the divergence of the solution for a lenticular drop at the contact line. The vapor flux is highest in the regions of the highest concentration gradient, i.e., at the edges. (b) Illustration of the contraction of an evaporating drop in the absence of contact line pinning. In this case the higher evaporation rate at the contact line is matched by a larger volume of liquid lost as the edge retreats. (c) The contraction and change in shape of an evaporating drop in the case that the contact line is pinned. Here there must be a flow of fluid from the center of the drop to the periphery to compensate for the accelerating rate of evaporation from the increasingly shallow-angled contact line.

Finally, we may also calculate the energies ΔW of the flotation and immersion capillary forces acting on particles.[19] The first of these arises from the deformation of the meniscus by the weight of the particles, and, for two identical particles, is given approximately by[20]

$$\Delta W_{\text{flotation}} \approx \gamma q^4 r^6 Ln[qL], \tag{2}$$

where γ is the liquid/vapor surface energy, r is the particle radius, L is their separation, and $q^{-1}=[\gamma/g\rho]^{1/2}$ is the capillary length, with ρ the fluid density and g the acceleration

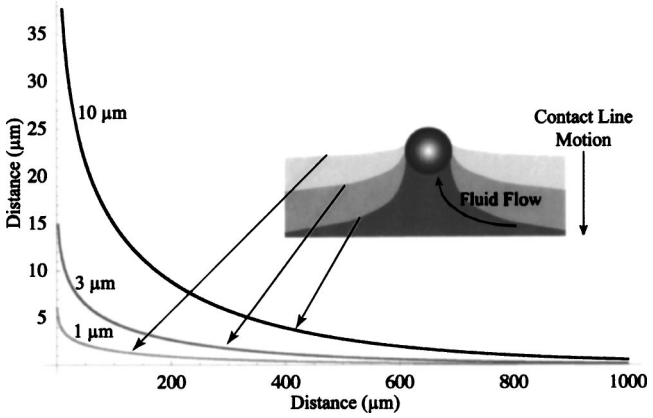

FIG. 4. Calculated profiles for a water contact line passing a pinning defect for effective defect sizes of 1, 3, and 10 μm. The defect, and hence the pinning force, effectively grows as the defect emerges from the contact line. The inset is a schematic of the contact line motion as the fluid passes the particle. The fluid flow to the pinning point occurs as a result of the mechanism illustrated in Fig. 3.

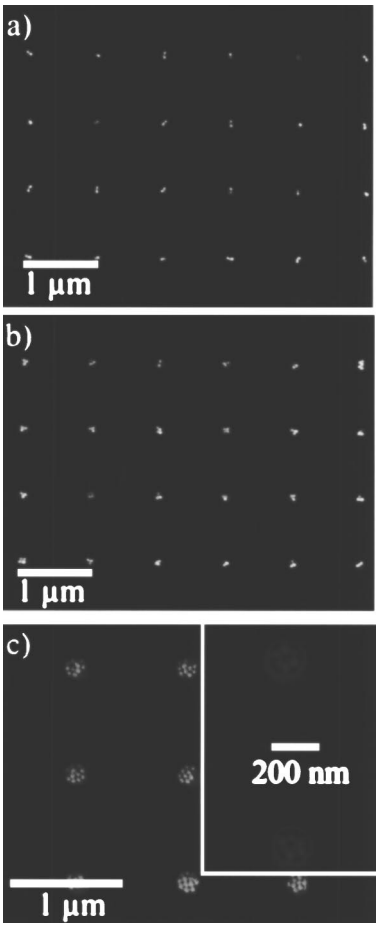

FIG. 5. SEM micrographs showing the effect of the particle-to-hole diameter ratio on the number of particles in each hole. (a) Two particles/hole. (b) Three particles/hole. (c) Many particles/hole. In this case the holes are deep enough to permit the particles to stack (inset). Note that the orientation of the particle dimers is random and therefore independent of the direction of the fluid flow.

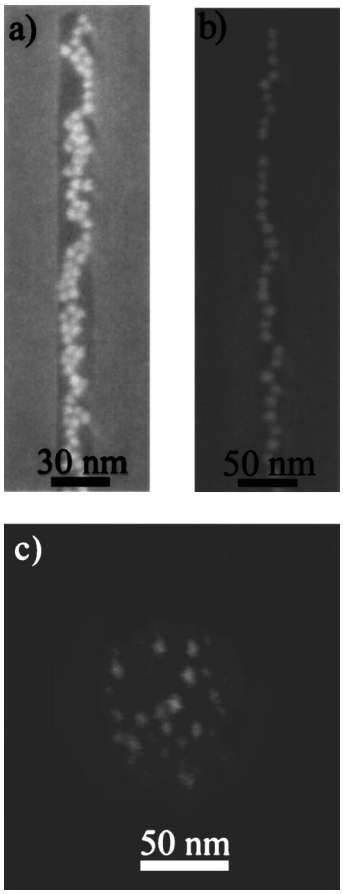

FIG. 6. 8 nm Au particles in (a) a 20 nm trench, (b) a 15 nm trench, and (c) a 100 nm hole. The organization of the particles is less controlled than for the larger particles, where the ratio of particle diameter to feature size can be more precisely controlled.

due to gravity. For $\gamma=50$ mN/m, $\Delta W_{\text{flotation}}$ is of order kT for $r=10\mu$ m, and, given the r^6 dependence, rapidly becomes insignificant for smaller particles. The second is also a result of meniscus deformation, and occurs as a result of the fluid wetting behavior in thin films, when, for example, the particles are confined by a surface (Fig. 1). It is given approximately by

$$\Delta W_{\text{immersion}} \approx \gamma r^2 Ln[qL]. \tag{3}$$

This remains large with respect to kT, even for particles as small as 1 nm, and, because of the r^2 dependence, is long range, with a characteristic capillary length of q^{-1}. In the bulk, the capillary length for water is approximately 2.7 mm, and remains relatively large (i.e. >1 μm), even in very thin (i.e., 25 nm) films.[21]

From this brief survey, we may thus conclude that the immersion forces acting between nanoparticles, or between nanoparticles and lithographically defined nanoscale surface topographies, meet our requirements and are capable of bringing nanoparticles together over relatively long distances and of confining them effectively.

MECHANISM OF LITHOGRAPHICALLY-DIRECTED FLUIDIC ASSEMBLY

The notion that the immersion capillary force can cause nanoparticles to assemble at a topographic feature relies on there being a thin liquid film containing a suitable concentration of nanoparticles very close by. Figure 2 is a scanning electron microscopy (SEM) micrograph of holes, approximately 100 nm in diameter on a 1 μm pitch, in resist, each of which contains approximately seven nanoparticles. There are no nanoparticles between the lithographically defined features. The nanoparticles were assembled from solutions with nanoparticle volume fractions of 0.0125% or 0.0006%, corresponding to interparticle spacings of 1 to 2.8 μm, respectively. The assemblages represent an increase in concentration of 10^4 to 10^5. The question is then: What mechanism leads to the concentration of nanoparticles at the lithographically defined features?

It has been observed that drying drops of suspensions, such as coffee, leave residues that are significantly darker or more concentrated at their perimeters. The reason for this has been elucidated recently,[22–25] and the basic mechanism is illustrated in Fig. 3. In brief, the equilibrium of the three-phase contact line of a liquid is normally determined by the Young

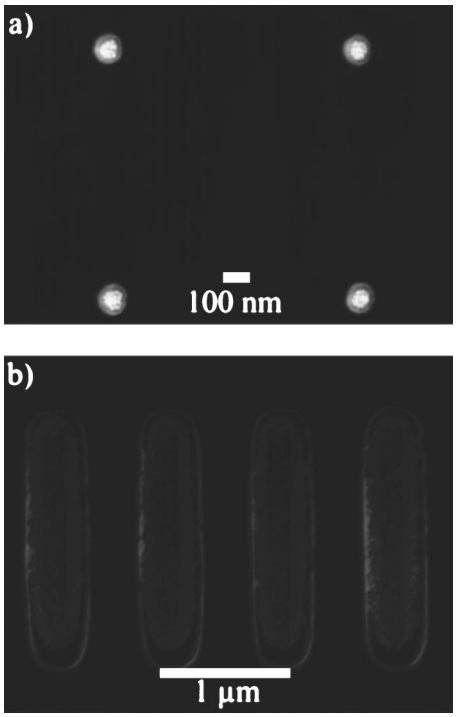

FIG. 7. SEM micrographs of 2 nm Au particles in (a) holes and (b) trenches. Note the separation of the particle aggregate from the trench walls. This is indicative of a final drying stage occurring after the liquid contact line has broken free of the lithographically defined feature.

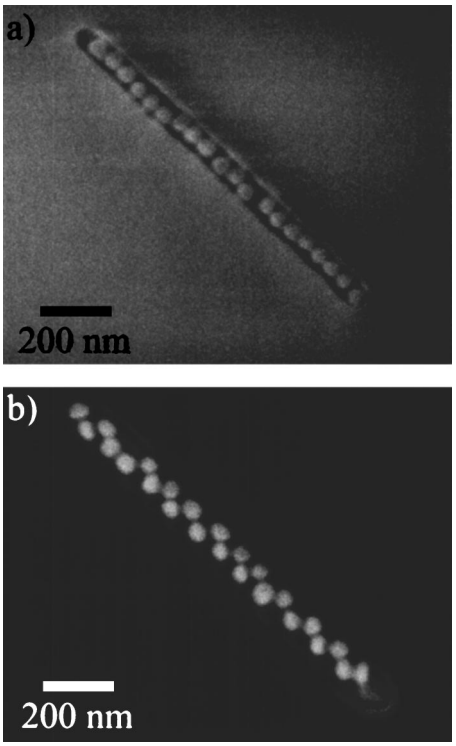

FIG. 8. SEM micrographs of 50 nm Au particles arranged in extended templates. The high degree of ordering exhibited, particularly in (b), is indicative that the particles are still able to reconfigure within the features for some time after they have arrived.

condition[26] and, when liquid evaporates from a drop, the drop will maintain a constant shape, by shrinking, as a consequence of that equilibrium [Fig. 3(b)]. However, if the contact line becomes pinned, then, as evaporation takes place, there must be a net flow of liquid toward the contact line [Fig. 3(c)] that carries the suspended particles to the contact line and concentrates them there. In the case that the accumulated particles exert a sufficient pinning force on the contact line, then the phenomenon of self-pinning occurs, leading to an even greater build-up of particles.

We may suppose, then, that the lithographically generated surface features act as pinning sites for the moving contact line. When the contact line passes a pinning site it is deformed[27] (Fig. 4), and it is this deformation that leads to a rapidly diverging evaporation rate and increase in fluid flow towards the pinning site. The fluid flow carries the nanoparticles with it, leading to the observed dramatic increase in particle concentration. As the interface continues to recede from the pinning site, the amount of deformation increases until, eventually, it breaks free.[28–31] Note that self-pinning must not occur, otherwise there would be an uncontrolled buildup of nanoparticles at the lithographically defined location.

The nanoparticles will be further concentrated and assembled into the features as a result of the immersion capillary force described earlier and secured by van der Waals and electrostatic forces to one another and the sides/base of the defined features. It is probable that, at least in some cases, there is a small volume of liquid retained in the feature that allows for further equilibration of the nanoparticle arrangement before drying is complete.[32]

RESULTS

The following results were obtained by allowing the contact line of various aqueous suspensions of Au nanoparticles to pass over a lithographically patterned surface. The velocity of the contact line was typically on the order of 10 μm/min and was controlled through natural or forced evaporation. It was observed that successful assembly only occurred for macroscopic water-substrate contact angles in the range 10° to 30°. We speculate that this represents the situation where there is sufficient interaction with the lithographically created features for the right degree of pinning to occur for the concentration mechanism to operate, but not so much that self-pinning occurs. In the case of assembly on normally hydrophobic resist surfaces, the contact angle was adjusted to the desired value by means of a short oxygen-plasma treatment.

Figure 5 is a series of SEM micrographs of 50 nm Au particles deposited into holes of differing diameters fabricated by electron-beam lithography in 60 nm thick (KRS-XE) resist. The number of nanoparticles in each hole is relatively well controlled and is determined geometrically by the ratio of the particle-to-hole diameters. It should be noted that

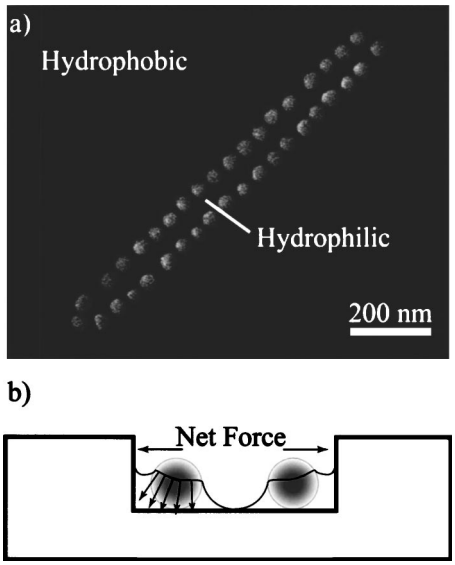

FIG. 9. (a) SEM micrograph of 50 nm Au particles arranged around the perimeter of a trench in resist (hydrophobic) on an SiO_2 surface (hydrophilic). (b) Schematic illustrating the contact line tilt that causes the nanoparticles to decorate the sides of the trench. If there is no difference in hydrophilicity between the bottom and sides of the trench then the particles are distributed randomly within it.

the orientation of the particle clusters is random and therefore not influenced by the direction of fluid flow, in contrast to the work of Yin and Xia.[15]

Figure 6 shows the assembly of 8 nm particles in SiO_2 templates. The ordering of the particles is relatively poor because of the large size of the features relative to the particles. Figure 7 shows the assembly of 2 nm particles—the individual particles are not resolved. There is no particle contamination of the areas surrounding the features, which suggests that the same assembly mechanism is operating at this particle size. We note also that there is clearly some shrinkage of the particle assembly within the feature. This lends credence to the idea that liquid is retained within the feature after the contact line has passed by and that there is a further drying step within the feature.

Particles may be assembled into templates having a variety of shapes, as illustrated by Fig. 8. Relatively complex particle arrangements can be obtained by controlling the template-to-particle size ratio. Again, the fact that the particles are so well ordered supports the hypothesis that the particles are still mobile after they are trapped in the features. Figure 9 shows particles organized into a relatively hydrophobic resist feature on a hydrophilic SiO_2 substrate. The choice of template sidewall and base materials offers an additional degree of freedom in controlling particle assembly.

In addition to spherical particles, the distribution of more complex nanostructures can be controlled by this technique. Figure 10 shows the assembly of nanotetrapods into trenches in resist. As the trenches become narrower, the orientation of the tetrapods becomes increasingly well-defined. We believe that assembly occurs through a combination of sliding and rotation [Fig. 10(b)].

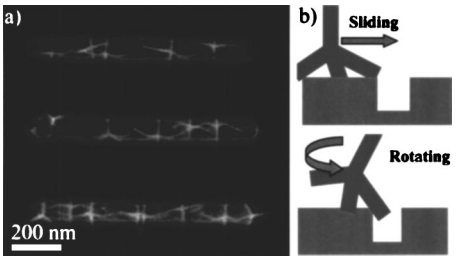

FIG. 10. (a) SEM micrograph of nanotetrapods assembled in trenches in resist. The trenches become wider from top to bottom and the tetrapod orientation becomes correspondingly less well controlled. (b) Schematic of proposed assembly mechanism: The tetrapods first slide across the surface until one foot is trapped and then rotate until a second is also captured. The tetrapods were dispersed in toluene.

Finally, in Fig. 11, we demonstrate the controlled, high-yield assembly of nanoparticles into the gap between prepatterned Au electrodes on an SiO_2 surface. Figure 11(c) shows preliminary electrical characterization data from such a structure. In this instance, because the Au electrodes are above rather than below the surface, the flow direction has an influence on the yield, as shown in Fig. 11(b). This is most probably a result of whether or not the structure is able to physically constrain the nanoparticle as the contact line moves past.

CONCLUSIONS

Lithographically defined templates together with the capillary forces present during evaporation of a liquid containing nanostructures provide the necessary conditions for the organization of those nanostructures. The key effect leading to high yield and high specificity is the concentration of the nanostructures at the lithographically defined location through pinning of the moving liquid contact line. Structures on multiple length scales from the nanometer to the macroscopic can be controlled by appropriate choice of nanostructure size and lithographic pattern. Adjustment of the relative

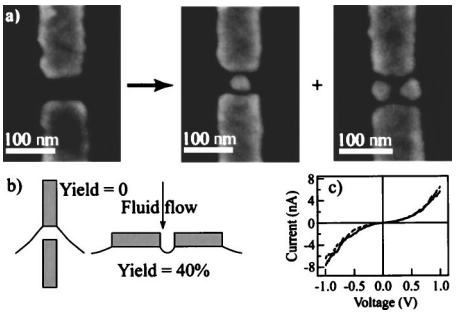

FIG. 11. (a) Sequence of SEM micrographs illustrating the assembly of single 30 nm Au particles between pairs of prepatterned Au electrodes. The electrodes provide sufficient topography to pin the fluid contact line and cause assembly. (b) However, in this case, because the electrodes are raised above the surface, the assembly only works when the fluid flow direction permits mechanical pinning of the particles. (c) Preliminary electrical measurement of the current/voltage characteristics of an electrode/nanoparticle assembly.

surface energies of the liquid, particle, and substrate provides additional degrees of freedom for controlling the ordering of the nanostructures.

We have demonstrated controlled positioning of particles as small as 2 nm in diameter—the same scale as individual protein molecules—with this technique, as well as that of complex nanostructures such as nanotetrapods, and nanoparticles of a wide variety of materials. In addition, we have created arrays of simple electronic devices with this method. This approach offers a straightforward and generally applicable method for integrating bottom-up solution-processed nanostructures with top-down lithographically prepared devices, and it has the potential to be scaled up to wafer size for many functional nanoelectronics and nanophotonics applications. It is also clear that this process is rich in interesting physics.

ACKNOWLEDGMENTS

This work was supported by DARPA Contract No. MDA972-98-C-0007.

[1]M. Brust and C. J. Kiely, Colloids Surf., A **202**, 175 (2002).
[2]C. A. Mirkin, Inorg. Chem. **39**, 2258 (2000).
[3]A. P. Alivisatos, Science **271**, 933 (1996).
[4]C. B. Murray, C. R. Kagan, and M. G. Bawendi, Annu. Rev. Mater. Sci. **30**, 545 (2000).
[5]X. Peng, U. Manna, W. Wang, J. Wickham, E. Scher, A. Kadaranchi, and A. P. Alivisatos, Nature (London) **404**, 59 (2000).
[6]L. Manna, D. J. Milliron, A. Meisel, E. C. Scher, and A. P. Alivisatos, Nat. Mater. **2**, 382 (2003).
[7]H. Grabert and M. H. Devoret, *Single-Charge Tunneling: Coulomb Blockade Phenomena in Nanostructures* (Plenum Press, New York, 1992).
[8]S. Sun, C. B. Murray, D. Weller, L. Folks, and A. Moser, Science **287**, 1989 (2000).
[9]S. A. Maier, M. L. Brongersma, P. G. Kik, S. Meltzer, A. A. G. Requicha, and H. A. Atwater, Adv. Mater. (Weinheim, Ger.) **13**, 1501 (2001).
[10]D. L. Klein, R. Roth, A. K. L. Lim, A. P. Alivisatos, and P. L. McEuen, Nature (London) **389**, 699 (1997).
[11]J. P. Spatz *et al.*, Adv. Mater. (Weinheim, Ger.) **14**, 1827 (2002).
[12]A. Bezryadin, C. Dekker, and G. Schmid, Appl. Phys. Lett. **71**, 1273 (1997).
[13]C. S. Lee, H. Lee, and R. M. Westervelt, Appl. Phys. Lett. **79**, 3308 (2001).
[14]Y. Yin, Y. Lu, B. Gates, and Y. Xia, J. Am. Chem. Soc. **123**, 8718 (2001).
[15]Y. Yin and Y. Xia, J. Am. Chem. Soc. **125**, 2048 (2003).
[16]S. H. Behrens and D. G. Grier, J. Chem. Phys. **115**, 6716 (2001).
[17]S. Biggs, P. Mulvaney, C. F. Zukoski, and F. Grieser, J. Am. Chem. Soc. **116**, 9150 (1994).
[18]S. Bhattacharjee, M. Eimelech, and M. Borkovec, Croat. Chem. Acta **71**, 883 (1998).
[19]P. A. Kralchevsky and K. Nagayama, Adv. Colloid Interface Sci. **85**, 145 (2000).
[20]V. N. Paunov, P. A. Kralchevsky, N. D. Denkov, and K. Nagayama, J. Colloid Interface Sci. **157**, 100 (1993).
[21]P. A. Kralchevsky and K. Nagayama, Langmuir **10**, 23 (1994).
[22]R. D. Deegan, O. Bakajin, T. F. Dupont, G. Huber, S. R. Nagel, and T. A. Witten, Nature (London) **389**, 827 (1997).
[23]R. D. Deegan, Phys. Rev. E **61**, 475 (2000).
[24]R. D. Deegan, O. Bakajin, T. F. Dupont, G. Huber, S. R. Nagel, and T. A. Witten, Phys. Rev. E **62**, 756 (2000).
[25]B. J. Fischer, Langmuir **18**, 60 (2002).
[26]P. G. de Gennes, Rev. Mod. Phys. **57**, 827 (1985).
[27]G. D. Nadkarni and S. Garoff, Europhys. Lett. **20**, 523 (1992).
[28]J. F. Joanny and P. G. de Gennes, J. Chem. Phys. **81**, 552 (1984).
[29]E. Raphael and P. G. de Gennes, J. Chem. Phys. **90**, 7577 (1989).
[30]J. F. Joanny and M. O. Robbins, J. Chem. Phys. **92**, 3206 (1990).
[31]M. E. R. Shanahan, Langmuir **11**, 1041 (1995).
[32]J. Aizenberg, P. V. Braun, and P. Wiltzius, Phys. Rev. Lett. **84**, 2997 (2000).